INSTITUTE OF PHYSICS PUBLISHING NANOTECHNOLOGY
Nanotechnology **17** (2006) S231–S239 doi:10.1088/0957-4484/17/11/S02

Vapour-transport-deposition growth of ZnO nanostructures: switch between *c*-axial wires and *a*-axial belts by indium doping

Hong Jin Fan[1,4], Bodo Fuhrmann[2], Roland Scholz[1], Cameliu Himcinschi[1], Andreas Berger[1], Hartmut Leipner[2], Armin Dadgar[3], Alois Krost[3], Silke Christiansen[1], Ulrich Gösele[1] and Margit Zacharias[1]

[1] Max Planck Institute of Microstructure Physics, Weinberg 2, 06120 Halle, Germany
[2] Interdisciplinary Center of Materials Science, Hoher Weg 8, Martin-Luther-University Halle, Germany
[3] Institute of Experimental Physics, Otto-von-Guericke University, 39016 Magdeburg, Germany

E-mail: hjfan@mpi-halle.de

Received 5 January 2006, in final form 21 February 2006
Published 19 May 2006
Online at stacks.iop.org/Nano/17/S231

Abstract
ZnO nanowires and nanobelts are two representatives of one-dimensional semiconductor nanomaterials possessing potential applications as optoelectronic and sensor devices. In this study, we applied a vapour-transport-deposition method to synthesize both types of nanostructures using relatively low temperatures (860 °C) by controlling the source materials. We found that the resulting product under similar growth conditions can be switched between [0001]-axial nanowires and $\langle 11\bar{2}0\rangle$-axial nanobelts simply by adding indium to the source. The former appear as ordered vertical arrays of pure ZnO while the latter are belts without spatial ordering. Both represent defect-free single crystals grown via the vapour–liquid–solid mechanism using nanosphere lithography-fabricated catalyst Au templates. Examination of the early growth stage suggests that the dissolution of In into Au influences the nucleation of ZnO at the solid–liquid interface, and subsequently defines the structure and crystallographic orientation of the nanobelts. The optical properties of both nanostructures are studied by photoluminescence and resonant Raman scattering, which indicate consistently that the doped nanobelts have a higher carrier concentration than the nanowires.

(Some figures in this article are in colour only in the electronic version)

1. Introduction

Since the pioneering work on ZnO nanowires by the Yang group [1] and on semiconducting metal oxide (including ZnO) nanobelts by the Wang group [2], the synthesis of one-dimensional (1D) nanostructures has been further developed using various techniques. Much effort is being paid to *in situ* control of the structure, morphology, position, and composition of nanomaterials during the growth. In the case of ZnO 1D nanostructures, a nanowire generally refers to a structure elongated in the [0001] direction (namely, *c*-axial) with a quasi-hexagonal cross section, in accordance with the growth

[4] Author to whom any correspondence should be addressed.

habit of wurtzite ZnO crystals. Nanobelts mainly refer to a growth elongated in $\langle 11\bar{2}0\rangle$ (*a*-axial) or $\langle 10\bar{1}0\rangle$ (*m*-axial) directions with rectangular cross sections [2, 3]. Applications of ZnO 1D nanostructures in different fields require different structure and orientations, and hence a desire for growth control.

Vapour-transport deposition (VTD) inside a horizontal tube furnace is a common method for the growth of low-dimensional nanostructures. Growth of needle-shaped ZnO whiskers was demonstrated as early as 1974 using a VTD method [4]. In recent years, a wide range of 1D semiconductor nanostructures including ZnO have been fabricated with this technique (see reviews in [5–7]). A successful growth is known to be sensitively dependent on such parameters like source type, substrate orientation, temperature, partial pressure of reactants, and catalyst size [8–13]. Such dependence not only enables the manipulation of 1D ZnO nanomaterial growth by choosing appropriate conditions to influence the growth kinetics or thermodynamics [12, 13], but is also useful in understanding the growth mechanism of nanocrystals. Similarly, it has been demonstrated by a number of groups that the morphology and composition of other non-ZnO nanomaterials, such as Si, Ge and their oxides [14–16], ZnS [17], and Al_2O_3 [18], are also strongly sensitive to the reaction temperature and substrate position in the VTD growth setup.

On the other hand, despite the large variety of the fabrication methods for ZnO 1D nanomaterial, the synthesizing conditions differ from system to system and from group to group, and correspondingly, so do the growth mechanisms discussed. For example, ZnO nanowires/nanoneedles can be obtained from evaporation and oxidation of Zn [10, 19, 20], $ZnAs_2$ [21], and $ZnCl_2$ [22] at low temperatures (<600 °C), and also by carbothermal reduction of ZnO powder at temperatures of 800–950 °C [9, 11, 12]. The latter technique allows a better control of Zn vapour concentration which is important when a patterned growth is concerned [9, 23]. In most cases, the morphology, size and alignment of the ZnO nanowires vary greatly with the reaction temperature [10, 24, 25], but in different degrees for different synthesizing configurations. Nanobelts are generally grown by high temperature (>1000 °C) evaporation of ZnO powder in the Wang group [8]. But the use of other sources in various temperature environments for the growth of belt-like structures have also been reported [24, 26–29]. In addition, when impurities are mixed into the source material during the VTD growth, more complex ZnO structures can be developed, for instance, nanohelix [30], nanorings [31], bridges [32], propellers [25], and nail-wire nanojunctions [33], depending significantly on temperature and amount of impurities used. Overall, the experimental conditions reported for the growth of ZnO 1D nanostructures are rather diverse and in some cases are discussed with inconsistent growth mechanisms.

In this paper, we demonstrate that, during the VTD growth of ZnO 1D nanostructures, the resulting product can be reproducibly switched from [0001]-axial nanowires to In-doped $\langle 11\bar{2}0\rangle$-axial nanobelts by adopting different types of sources while keeping all other conditions constant. We will show early growth stages, which proves that the nucleation and crystallization behaviours are different at such early stages. The influence of the possible presence of an In–Zn–Au ternary alloy phase at the beginning will be discussed. The optical properties are investigated using photoluminescence and resonant Raman scattering and they are discussed in a comparison.

2. Experimental details

2.1. Template fabrication

Au dot templates on GaN(0001)/Si (grown by metal organic vapour phase epitaxy) substrates were fabricated through a modified nanosphere lithography (NSL) technique [34]. First, Si substrates were cleaned by immersing in $H_2O/NH_4OH/H_2O_2$ (5:1:1 at 80 °C for 15 min). Then suspensions of monodisperse spherical polystyrene particles (10 wt% in water, diameter 508 nm, Microparticles GmbH, Berlin, Germany), further diluted with equal amounts of methanol containing 0.25% Triton x-100, were spin coated onto the Si substrates. The spin speed was adjusted so that mainly hexagonally closed packed bilayers of the spheres were formed on the Si substrate. Second, in order for stabilization of the particle mask a ≈50 nm thick Au film was deposited by thermal evaporation on top of the bilayers. Next, the Si substrates were slowly immersed into deionized water to separate the stabilized particle mask. The membranes were then transferred onto the surface of GaN by immersing the substrate into the solution and lifting up the substrate together with the membrane. Subsequently, a thin gold film (≈1.5 nm) was deposited onto the substrates through the membrane masks. Finally, the masks were removed by dissolution in CH_2Cl_2 in an ultrasonic bath for 2 min, leaving the gold nanodiscs, ∼30 nm in average size, on the substrate surface.

2.2. Growth of nanowires and nanobelts

Growth of ZnO nanostructures was conducted inside a double tube furnace system through the VTD method (see figure 1). The growth system comprises a standard quartz tube furnace (Carbolite, inner tube diameter: 50 mm), vacuum adaptors, a gas flow controller, an oil-free pump station, and a needle valve. In order to obtain a sufficient Zn vapour pressure, the source materials and substrates were put in a small alumina tube (inner diameter: 15 mm). For the growth of epitaxial nanowire arrays, a mixture of ZnO + C powder (1:1 wt%) was used as source and located at position A in figure 1 (referred to as the 'A' experiment). For the growth of nanobelts, an additional alumina boat filled with In_2O_3 + C powder (1:1 wt%) was put at position B (referred to as the 'A + B' experiment). The Au coated GaN/Si substrates were located near the open end of the small alumina tube. A constant Ar gas flow (25 sccm) was directed into the small reaction tube by another small alumina tube. No additional O_2 gas was introduced since the residual/leaky air in our setup, with a partial pressure of $\sim 10^{-3}$ mbar, provides sufficient oxygen from thermodynamics point of view, in agreement with the conclusion by Park *et al* [13]. Indeed, when we mixed additional oxygen (1%) into the pure Ar, the ZnO reduction was significantly suppressed and no growth of nanowire was observed. The system was kept at the peak temperature for 25 min, and then cooled down naturally to room temperature.

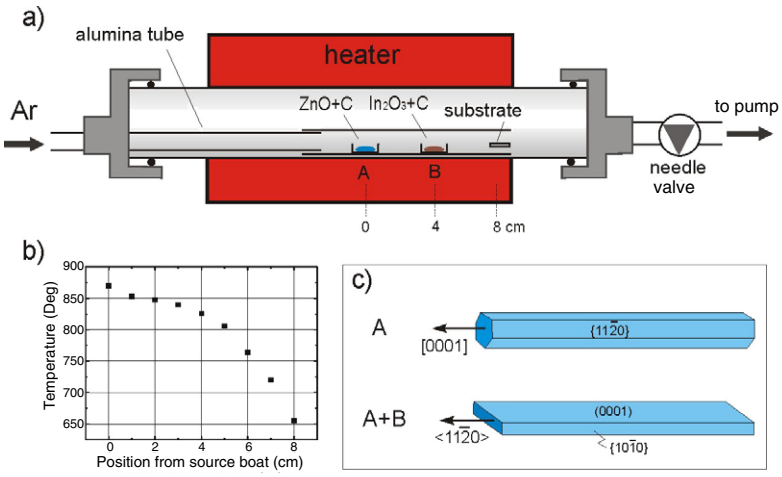

Figure 1. (a) Experimental setup for the growth of ZnO 1D nanostructures inside a quartz tube horizontal furnace. Both the source powder and substrate were located inside the reaction alumina tube, where their relative distances are labelled. (b) Temperature profile inside the reaction tube as measured using a thermocouple. (c) Schematic diagrams of the 1D nanostructure obtained under different growth conditions: *c*-axial nanowires when only ZnO + C source was used at position A; *a*-axial nanobelts when both ZnO + C (at position A) and In_2O_3 + C (at position B) sources were used.

Figure 1(b) shows the temperature profile of the furnace which is 860 °C at the centre and 650 °C at the substrate position. Note that we previously used a modified setup, which is a vapour-diffusion-deposition process, to grow ordered arrays of ZnO nanowires [23] and submicron-thick pillars on GaN/Si substrates [35].

2.3. Characterizations

The structure and composition of the nanostructures were investigated using scanning electron microscopy (SEM, JEOL JSM-6300F), transmission electron microscopy (TEM, Philip CM20T), and high resolution TEM (HRTEM, JEOL JEM-4010). The selected area electron diffraction patterns (SAEDs) and energy dispersive x-ray (EDX) spectra were obtained using a Philips CM20FEG TEM. Room temperature photoluminescence was excited by the 325 nm line of a He–Cd laser and detected by a nitrogen cooled charge-coupled device (CCD) camera. For the UV resonant Raman scattering, the samples were excited by the 325 nm line of a He–Cd laser and the spectra were collected by a LabRam HR800 UV spectrometer (Horiba Jobin Yvon) equipped with a liquid nitrogen cooled CCD detector (2048 × 512 pixels) and a 2400 grooves mm^{-1} grating. All spectra were obtained at room temperature in a backscattering geometry with 60 s accumulation and a laser spot size of about 1 μm.

3. Results and discussion

3.1. Overview of the result

Figure 1 shows the setup used for the growth of ZnO 1D nanostructures. Except for the In_2O_3 + C source boat, all the other conditions, including the substrates, were kept the same. A brief diagram of the result is shown schematically in figure 1(c). When only the ZnO + C source was used at position A, vertical arrays of ZnO nanowires were obtained growing along the [0001] direction and with hexagonal cross sections. However, if both ZnO + C and In_2O_3 + C were used at position A and B, respectively, the major product was randomly oriented ultralong nanobelts which covered the whole substrate surface evenly. Our analysis shows that the composition of the nanobelts was ZnO doped with indium (the atomic percentage of In, defined as In/(In + Zn), was 4–6 at.%) and the growth was along ⟨11$\bar{2}$0⟩ directions. A detailed comparison is presented in table 1. We repeated the experiments more than ten times and found that it is a reproducible phenomenon. At least two conclusions can be drawn from table 1: first, vertical aligned ZnO nanowires within long-range ordering can be easily realized by combining catalyst templates and the VTD technique, and we established a new method for growing ⟨11$\bar{2}$0⟩-axial ZnO nanobelts at relatively low source temperatures of 860 °C compared to 1300–1400 °C used in the Wang group [3]; second, the sharp difference between the results of the 'A' and 'A + B' experiments implies that indium plays the major role in defining the crystallographic orientation of the nanobelts, in addition to providing the dopant. In the following we examine the two structures in more detail.

Table 1. Comparison of the results from 'A' and 'A + B' experiments.

	'A' experiments	'A + B' experiments
Sample morphology	Vertical array of nanowires	Randomly oriented nanobelts
Composition	Pure ZnO	ZnO doped with In
Growth direction	[0001]	⟨11$\bar{2}$0⟩
Growth rate	Low	High
Length-to-width ratio	10–40	∼120

3.2. [0001]-axial nanowires

Figure 2 demonstrates two examples of the ZnO nanowire arrays which were grown with different Zn vapour concentration, which influences the diameter of the wires. The vertical alignment and periodic ordering of the wires was found

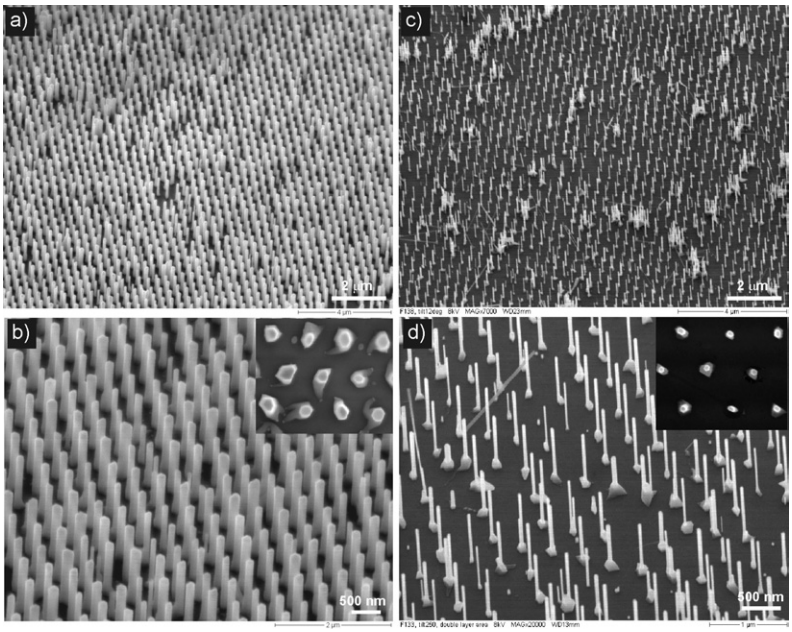

Figure 2. SEM images of the nanowire arrays grown using only ZnO + C source. ((a), (b)) Nanowires of diameters ∼140 nm; ((c), (d)) nanowires of diameters ∼50 nm. The insets are the corresponding top views of the wires showing their quasi-hexagonal ends.

to be present on a large scale for both cases. A single wire grows mainly from each Au site. Some stripes and empty sites are present in analogy to defects in a crystal lattice; these are mainly due to the size inhomogeneity and evaporation of the polystyrene spheres. But this shortcoming is surely improvable by upgrading the NSL technique, as demonstrated by other groups [36, 37]. The hexagonal ends of the wires (see insets) indicate that their main axis is along [0001]. The mean diameter of the ordered nanowires is ∼50 nm in figures 2(a), (b) and ∼140 nm in figures 2(c), (d) (wires growing from Au stripes were not counted). The nanowires are completely perpendicular to the GaN surface, as expected for epitaxial growth. As proved before [23, 38], the GaN(0001) layers are ideal substrates for the fabrication of highly ordered *c*-axial ZnO nanowires.

Some reports have been published on the NSL approach for the growth of hexagonal-patterned ZnO nanowire arrays on *a*-plane sapphire [36, 37, 39], which all show additional inclined wires. Here, we applied the NSL technique on GaN substrates to achieve ordered arrays of individual nanowires with a truly vertical alignment. In our experiments, the use of the small tube and relatively low substrate temperatures is the key to the successful growth of arrays of single nanowires at individual Au sites. The small alumina tube works as a spatial confinement to maintain a sufficiently high local vapour concentration near the substrates, so that the temperatures could be effectively lowered to reduce the thermal-induced diffusion of the small Au dots (⩽30 nm). In this way, the separation of the Au discs into smaller dots [23, 40] can be avoided, and hence, only one wire grows out of the disc.

The single crystallinity and VLS epitaxial growth of the ZnO nanowires were verified by cross-sectional TEM analysis. Figure 3(a) shows a low-magnification view of two ≈30 nm diameter nanowires. In addition to the vertical alignment, one can readily see the Au particles present at the tips of

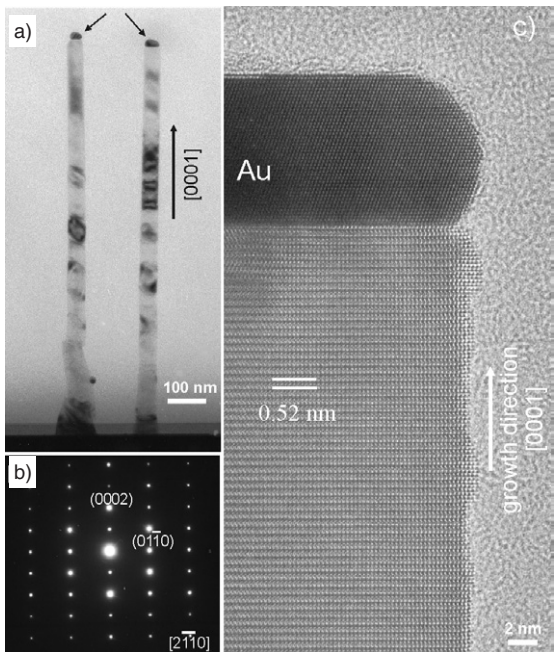

Figure 3. TEM images of the nanowires. (a) A cross-sectional view of two nanowires, showing their vertical alignment and the presence of Au particles on the wire tips. (b) SAED pattern recorded from one nanowire, confirming the axes direction along [0001]. (c) HRTEM image recorded near the tip of one wire, revealing the lattice structures of both Au and ZnO.

the nanowires. This confirms the growth mechanism to be VLS. The SAED pattern in figure 3(b) and the HRTEM image in figure 3(c) confirm that the nanowires are wurtzite single crystals with the main axes along the [0001] direction. In figure 3(c), the crystal perfection and atomic arrangement of both ZnO and Au, as well as an orientation relationship of

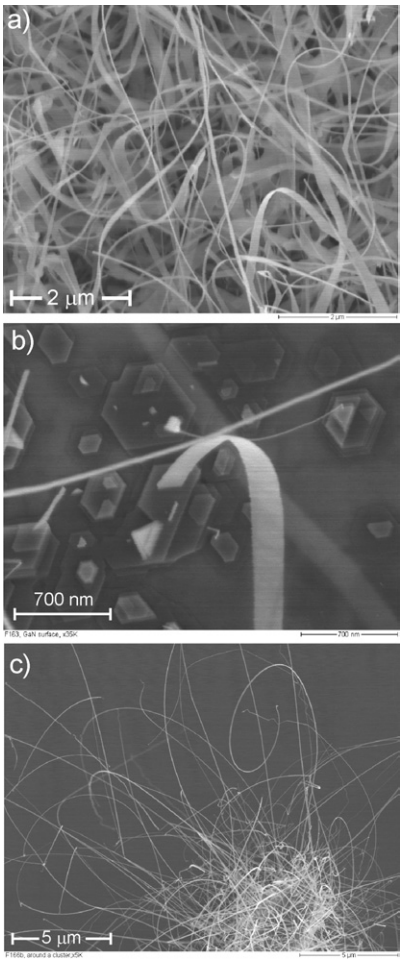

Figure 4. SEM images of the ZnO nanobelts grown using the source of ZnO + C at position A and In_2O_3 + C at position B. (a) Nanobelts grown from individual Au nanoparticles. (b) The same sample as (a) but the area with a smaller coverage of belts, showing a single nanobelt grown from a quasi-hexagonal base. (c) Nanobelts grown from a gold-covered SiO_2 particle on Si substrate.

Au(111) ∥ ZnO(0002), can be identified. The roughness of the nanowire surface is no more than four atomic layers of the coverage. The lattice distance for the (0002) plane determined here is 0.52 nm, comparable to that for bulk ZnO.

3.3. ⟨11$\bar{2}$0⟩-axial nanobelts

In 'A + B' experiments, the position of the In_2O_3 source was carefully chosen, so that on the one hand a small amount of In vapour can be produced while on the other hand the possible formation of ZnO–In_2O_3 complex superstructures [32] was avoided. Figure 4 shows example SEM images from the results of a number of repeated 'A + B' experiments. The substrate in figures 4(a), (b) was GaN decorated with Au dots via NSL. These nanobelts have a typical length of ∼20 μm after a 25 min growth, nearly ten times longer than the nanowires when only a ZnO source was used. They have widths in the range 100–220 nm. Most of the nanobelts are smooth along their lengths, but a small amount of zigzag nanobelts was also observed. In fact, we realized that the formation of the nanobelts is substrate independent: we found very similar results when using different substrates of Si, SiO_2, and GaN while under the same growth conditions. Growth of the nanobelts was also catalysed by Au, since no growth was observed at places without Au covering (see figure 4(c)), and catalyst nanoparticles were indeed observed at the tips of the belts. Unlike the vertical nanowires in figure 2, the nanobelts cover the whole substrate surface evenly with random orientation. This is unsurprising since the growth direction of the nanobelts is along [11$\bar{2}$0], so no epitaxial growth is expected on the (0001)-oriented GaN surface. On the other hand, if a substrate with in-plane lattice matching ZnO [0001] and out-plane lattice matching ZnO [11$\bar{2}$0], e.g., γ-$LiAlO_2$ (100) [41], would be used in our 'A + B' experiments, we expect that vertically aligned arrays of *a*-axial nanobelts might be obtained, similarly to the *c*-axial nanowire arrays in figure 2.

A TEM image of three smooth nanobelts is shown in figure 5(a), from which the thickness is estimated to be about 10 nm. The SAED pattern (inset in figure 5(a)) confirms that the nanobelts are single crystals growing along ⟨11$\bar{2}$0⟩, with ±(0001) top and bottom surface, and ±(01$\bar{1}$0) side surfaces. The nanobelts grew also via the VLS mechanism, as indicated by the Au tips (inset of figure 5(a)). EDX spectra (figure 5(b)) taken from randomly selected belts show the presence of In, 4–6 at.%, besides the major content of Zn and O, as well as Au near the tip shown in the inset of figure 5(a). This implies that In atoms are doped within the ZnO nanobelts. The HRTEM image in figure 5(c) shows clearly the smooth and sharp surface, and its single-crystal hexagonal structure. The nanobelts in the present work are free of twins or dislocations, which is consistent with the undoped *a*-axial ZnO nanobelts reported by Kong and Wang [3], but different from the nanorings [42] and bicrystal nanobelts [43, 44] in which local segregation of impurity ions induces planar defects. In particular, the atomic percentage of indium in [42] was nearly 50%, much higher than that (4–6%) of the nanobelts herein. This suggests that in our case the In dopant substitutes Zn lattice sites.

As for the zigzag nanobelts, they are also *a*-axial single crystals. Figure 6 shows TEM images of one zigzag belt. The angles at the kinks are always 120° (see figures 6(a) and (b)). The corresponding SAED pattern enclosing three kinks confirms the single-crystallinity of the belts (the splitting of the high-index points is due to a bending effect), and the top surfaces of the belts are (0001) planes. HRTEM images show that all the segments grow along the equivalent ⟨11$\bar{2}$0⟩ directions (see figure 6(c)), and the atomic structure is coherent at the kinks, where the belts switch to equivalent crystallographic directions without involving twins or stacking faults (see figure 6(d)). EDX spectra (not shown) indicate that these zigzag belts are also In doped. Interestingly, these zigzag nanobelts are similar in structure and orientations to the 2D ZnO nanodendrites we reported before [45, 46], which were formed by the oxidation of polyhedral Zn microcrystals in air.

3.4. Early growth stage of the nanostructures

Based on the above results, it appears that a switching from *c*-axial wires to *a*-axial belts is related to the In doping. In order to prove that, we examined the early growth stages of

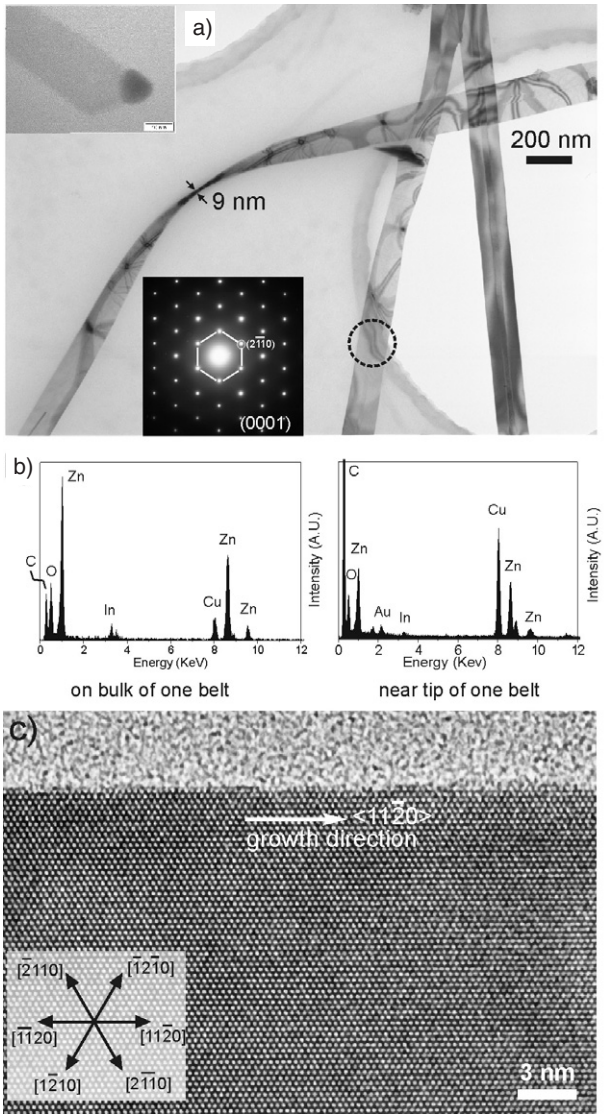

Figure 5. TEM images of the straight nanobelts. (a) An overview of three nanobelts. Top inset: one nanobelt showing the Au tip. Bottom inset: SAED pattern recorded from the circled area. (b) EDX spectra. Left: from the circled area in (a); right: near the tip (inset of (a)). The carbon and copper signals are from the TEM grid. (c) HRTEM image of part of one nanobelt, showing its single-crystallinity and atomically clean surface, as well as the growth direction along $\langle 11\bar{2}0\rangle$. The inset illustrates the six equivalent directions within the (0001) plane.

both structures. Figure 7(a) shows the result of a similar 'A' experiment to that in figures 2(c), (d), except for a shorter growth time (∼10 min). Individual pyramids of ZnO are seen, with some short rods tending to grow up vertically out of the substrate surface. This indicates a heteroepitaxial nucleation of ZnO on GaN, so that the pyramids and the subsequent nanowires are [0001] orientated. In contrast, the ZnO nanobelts in their early growth stage show a significantly different morphology. Figure 7(b) is the result after a 15 min 'A + B' experiment. Nearly no vertically aligned 1D structure was observed. Instead, two-dimensional nucleation seems to be favoured at the beginning, forming quasi-hexagonal pads with much larger size than those pyramids in figure 7(a). Sheet-like structures then extend out either laterally from the sides of the pads, or from the top of the pads (see figure 4(b)). An example of the embryo of the nanobelts is given in figure 7(c), which shows clearly the starting point of belt structure from the side of the hexagonal pads. Interestingly, the whole embryo is a single-crystal entity with ±(0001) top and bottom flat faces, as seen from the corresponding diffraction pattern in figure 7(c) as well as from HRTEM examinations (data not shown). The EDX spectrum also reveals the presence of indium in the embryo with a similar atomic percentage as in the nanobelts.

3.5. The growth mechanism

For the bottom-up vapour-phase growth of 1D structure of nanomaterials (especially defect-free single crystals), the most-accepted growth models are VLS and vapour–solid (VS). In VLS, the driving force for the growth is the precipitation and nucleation at the liquid–solid interface, in which the size of the growing 1D structure depends on the composition and size of the liquid droplet. In VS, the 1D growth is mainly controlled by kinetics, for which the temperature and the supersaturation ratio are two dominant processing factors in affecting the morphology of the products [8]. Both mechanisms have been widely suggested for the growth of ZnO nanowires or nanobelts. In our study, since the Au is mandatory for the formation of both nanostructures and a Au tip does appear at their ends, we believe that VLS is the dominant mechanism, as shown schematically in figure 8. For the vertically aligned wire, the growth seed is a (0001)-oriented ZnO pyramid or hexagonal column which is formed through Zn precipitation and oxidation (figure 8(a)). However, the nanobelt starts from the side faces of a hexagonal-shaped seed, and proceeds under the guidance of the alloy tip (figure 8(b)).

The question is: why does the structure change from wire in 'A' experiments to belt in 'A + B' experiments? In similar VTD experiments, Jie *et al* [28] also obtained In-doped ZnO nanobelts by high temperature (1400 °C) evaporation of In_2O_3 + ZnO powder, and Fang *et al* [29] grew Sn-doped ZnO nanobelts on a Sn-coated substrate where the ZnO molecules were generated by low temperature (700 °C) evaporating Zn powder in a humid Ar gas flow. It might be inferred from these experiments that the VLS formation of belt-like ZnO nanostructure is related to the element doping. In order for a crystal to switch from one crystallographic structure [47] or orientation [3] to another, a key parameter is the energy difference which determines the growth condition necessary for controlled nucleation and/or growth. As the ZnO(0001) faces are the highest-energy low-index planes (as shown by theoretical calculations [48, 49]), a fast growth along [0001] is thermodynamically favoured over $\langle 11\bar{2}0\rangle$, in agreement with the growth habit of ZnO thin films and nanowires. Kong and Wang [3] obtained *a*-axial ZnO nanobelts by controlling the growth kinetics in a way (thermal evaporation of ZnO powder in vacuum followed by vapour transport) that the energy barrier between the (0001) plane and $(11\bar{2}0)$ planes was somehow overcome. Our study on early growth stages of 1D ZnO nanostructures (figure 7) clearly shows the different nucleation behaviour for *c*-axial nanowires and *a*-axial nanobelts. Indium vapour generated by carbothermal reduction of In_2O_3 [50] can dissolve into Au up to a solubility of ≈24 at.% at about

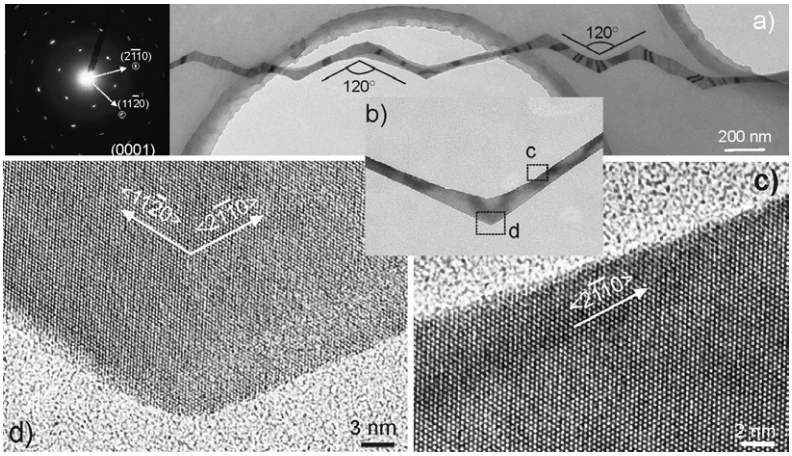

Figure 6. TEM images of the zigzag nanobelts. (a) An overview of a single zigzag nanobelt. The turning angles are always 120°. Inset: SAED pattern of an area including several segments. The hexagonal symmetry indicates that the top surface is a (0001) plane. (b) Magnified view of one turning point. (c) HRTEM image of the indicated straight section in (b), showing the atomically sharp surface growth direction along $\langle 11\bar{2}0 \rangle$. (d) HRTEM image of the indicated area in (b), showing the lattice coherency within the (0001) plane and absence of twins.

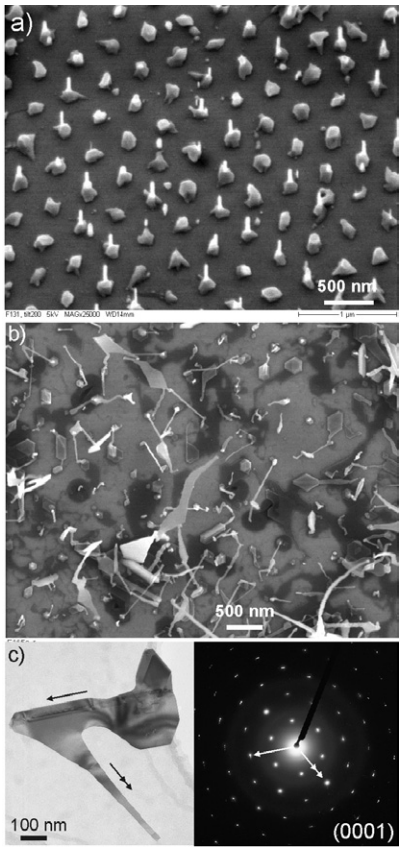

Figure 7. The early growth stage of the ZnO 1D nanostructures using separated Au nanoparticles as growth templates and catalyst. (a) 20° tilted view of the sample after a 5 min 'A' experiment. (b) Top view of the sample after a 15 min 'A + B' experiment. (c) TEM image and the corresponding diffraction pattern of an embryo in (b). The arrows indicate the growth orientation of the branches in equivalent $\langle 11\bar{2}0 \rangle$ directions.

650 °C. Nevertheless, the In content in Au is expected to be much lower than Zn, since the In vapour concentration is much lower than that of Zn (we did not observe any growth in 'B' experiments when only $In_2O_3 + C$ source was used). Therefore, we propose that a Au–Zn–In ternary phase gives rise to a certain strain to change the surface free energy, so that the nucleation behaviour of ZnO at the solid–liquid interface upon supersaturation and oxidation of Zn is modified. Such ternary alloy continues at the tip of the nanobelt during its elongation (see figure 8(b)), so as to maintain a stable belt-structure. As for the kinking of the zigzag belts, it is probably due to some thermal or strain instability at the liquid–solid interface, which can occur without involving much energy since the free energy is the same for the equivalent $\{11\bar{2}0\}$ planes. Similar kinkings in equivalent lattice planes were also observed in Si nanowires [51].

Furthermore, as discussed by Jie *et al* [28] for their In-doped ZnO nanobelts and Kar *et al* [52] for their nanometre- to micrometre-wide ZnS belts, direct impingement of Zn and In vapour atoms onto the side faces of the growing nanobelts could also occur, giving rise to lateral growth in the $\{10\bar{1}0\}$ faces via the VS mechanism. This explains why some of the nanobelts have widths larger than the catalyst Au tip.

3.6. Optical properties

Photoluminescence (PL) and resonant Raman scattering (RRS) measurements were carried out in order to check the optical quality of both nanostructures and the possible effect of indium doping. In order to avoid signals from GaN, the nanowires (50–80 nm in diameter) and nanobelts were grown on SiO_2-coated Si substrates.

Figure 9 shows the room temperature PL spectra for both structures. Examination of different places of the substrate gave consistent spectra. Relatively narrow near bandgap emissions (NBEs) are seen at about 377 nm. The NBE peak of the nanobelts redshifted by about 26 meV (3 nm) relative to the emission of the wires. Such a redshift could be due to optical bandgap narrowing effect caused by impurity-induced potential fluctuations, as previously observed by Kim *et al* [53] in their optical absorption study of In-doped ZnO film, and Jie *et al* [28] in the low temperature PL measurement of In-doped ZnO nanobelts. This is reasonable as the indium doping will increase the carrier concentration in the nanobelts compared

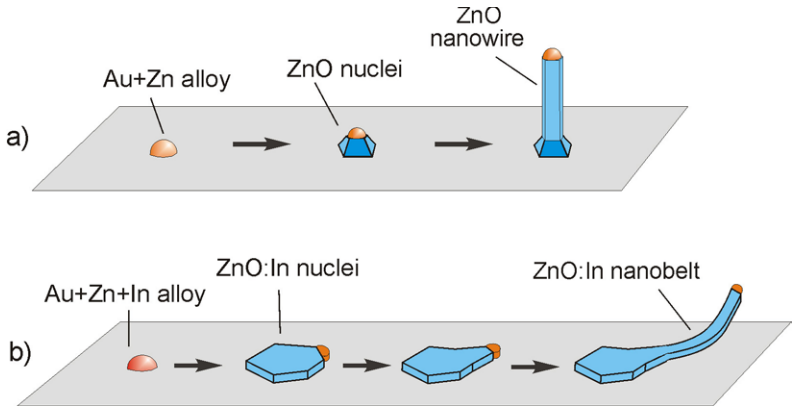

Figure 8. Proposed growth processes for the nanowire (a) and nanobelt (b). The main difference is that the nanowire grows upwards on the top (0001) plane of a ZnO columnar/pyramidal nuclei, whereas the nanobelt grows mainly from the side faces of a quasi-hexagonal ZnO:In pad (dimensions not to scale).

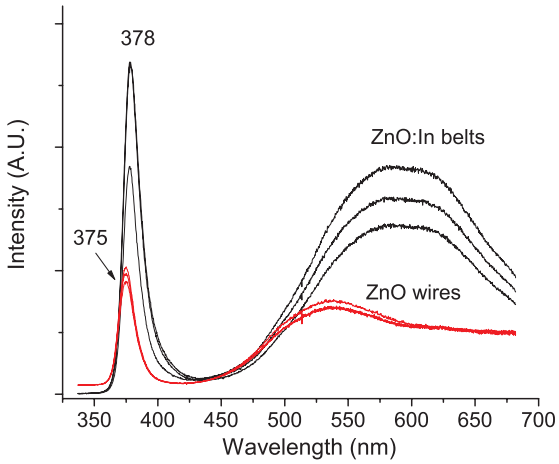

Figure 9. Room temperature photoluminescence spectra of the nanowires (lower three branches) and In-doped nanobelts (upper three branches). For this measurement both of the nanowires and nanobelts were grown on an SiO_2 layer.

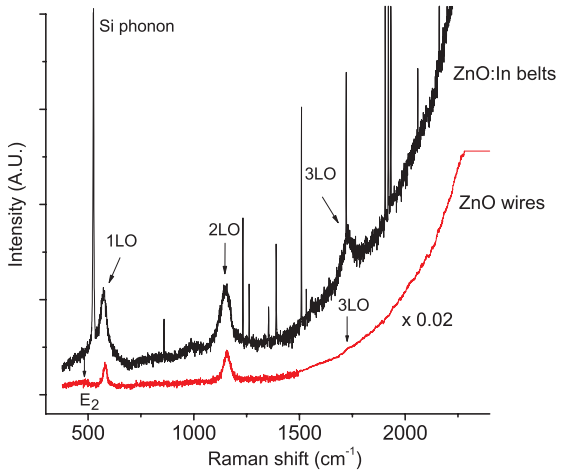

Figure 10. Room temperature resonant Raman spectra of the nanowires (lower branch) and In-doped nanobelts (upper branch). The intensity of the spectrum over 1500 cm^{-1} was multiplied by 0.02 for the nanowire sample. Multi-LO lines are observed on the high energy shoulder of the PL. The unlabelled sharp peaks from the nanobelts are plasma lines. For this measurement both of the nanowires and nanobelts were grown on an SiO_2 layer.

to the undoped nanowires. Another feature in figure 8 is the broad bands which are dominated by green emissions (500–540 nm) for the wires and yellow emission (580–620 nm) for the belts. As visible emissions in ZnO are usually caused by intrinsic defects (e.g., oxygen deficiencies and interstitials) or impurities, it is suggested that the two structures consist of different types of defects/impurities. As also observed in [28], the difference in the visible emission centre could be related to the In impurity in the nanobelts.

RRS spectra of both samples were measured at room temperature using a UV micro-Raman spectrometer. As shown in figure 10, Raman peaks due to multi-longitudinal optical (LO) phonon scattering [54] are observed for both structures on the high-energy tail of the PL. For the nanowires the 1LO and 2LO peaks can be seen, centred at 582 and 1158 cm^{-1}, with bandwidths of ∼12 and 42 cm^{-1}, respectively. A weak but recognizable 3LO line is also observed. For the nanobelts the first triple-order LO lines clearly appear at 572, 1152, and ≈1730 cm^{-1}, with bandwidths of ∼38, 80, and 50 cm^{-1}, respectively. The energies of these multi-LO lines are consistent with previously reported values of bulk ZnO [54], thin films [55] and nanowires [56]. According to the Raman selection rules for wurtzite crystals, the LO line could be an A_1 or E_1 mode, whose frequencies are different by ≈10 cm^{-1}, depending on scattering geometry. In our case, it is not possible to distinguish the A1 mode and E1 mode in the Raman spectra since the random alignment of the wires and belts grown on SiO_2 layers (images not shown) make the samples effectively isotropic.

The intensities of the multi-LO lines of our sample are lower than those of ZnO nanowires by Ng *et al* [56]. This is probably because our samples, grown at a relatively low temperature, contain a higher density of defects/impurities. Indeed, the PL spectra of our samples show much stronger defect-related visible emissions than those in [55]. The existence of defects in our samples could also account for the significant broadening of the phonon linewidths compared to the theoretical prediction of $9n$ (cm^{-1}) for nLO [54].

In their study of RRS of highly conductive ZnO layers, Zalamai *et al* [57] showed that the intensity ratio of 3LO

to 2LO (I_{3LO}/I_{2LO}) increases with the carrier concentration. In our case, the I_{3LO}/I_{2LO} in the nanowires is much lower than that in the nanobelts. This might imply a higher carrier concentration of the former than the latter, as consistent with the PL result in figure 9.

4. Conclusion

We demonstrated that, in the vapour-transport-deposition growth of ZnO nanostructures, it is possible to obtain both [0001]-axial nanowires and $\langle 11\bar{2}0\rangle$-axial nanobelts using similar conditions but different source type. The former appear as ordered vertical arrays of pure ZnO while the latter are In-doped nanobelts without spatial ordering. Both are defect-free single crystals grown via the VLS mechanism using catalyst Au templates. The origin of the switch in structure and orientation from nanowires to nanobelts is not fully understood at the moment. By studying their early growth stage, we proposed that the indium plays the significant role in defining the structure and crystallographic orientation of the nanobelts via influencing the alloying and nucleation at the liquid–solid interface of the growth front. Results of the photoluminescence and resonant Raman scattering imply that the doped nanobelts have a higher carrier concentration than the nanowires, although both contain certain amount of structural defects.

Acknowledgments

We thank M Hopfe and V Talalev for technical assistance with cross-sectional TEM sample preparation and PL measurement, respectively.

References

[1] Huang M H, Mao S, Feick H, Yan H Q, Wu Y Y, Kind H, Weber E, Russo R and Yang P D 2001 *Science* **292** 1897
[2] Pan Z W, Dai Z R and Wang Z L 2001 *Science* **291** 1947
[3] Kong X Y and Wang Z L 2003 *Nano Lett.* **3** 1625
[4] Matsushita T, Dodaira K, Saito J and Yoshida R 1974 *J. Cryst. Growth* **26** 147
[5] Wang Z L 2004 *J. Phys.: Condens. Matter* **16** R829
[6] Yi G C, Wang C and Park W I 2005 *Semicond. Sci. Technol.* **20** S22
[7] Fan Z Y and Lu G C 2005 *J. Nanosci. Nanotechnol.* **5** 1561
[8] Dai Z R, Pan Z W and Wang Z L 2003 *Adv. Funct. Mater.* **13** 9
[9] Yang P D, Yan H, Mao S, Russo R, Johnson J, Saykally R, Morris N, Pham J, He R and Choi H J 2002 *Adv. Funct. Mater.* **12** 323
[10] Lyu S C, Zhang Y, Lee C J, Ruh H and Lee H J 2003 *Chem. Mater.* **15** 3294
[11] Banerjee D, Lao J W, Wang D Z, Huang J Y, Steeves D, Kimball B and Ren Z F 2004 *Nanotechnology* **15** 404
[12] Song J, Wang X, Riedo E and Wang Z L 2005 *J. Phys. Chem.* B **109** 9869
[13] Park J H, Choi Y J and Park J G 2005 *J. Cryst. Growth* **280** 161
[14] Pan Z W, Dai Z R, Xu L, Lee S T and Wang Z L 2001 *J. Phys. Chem.* B **105** 2507
[15] Pan Z W, Dai S, Beach D B and Lowndes D H 2003 *Nano Lett.* **3** 1279
[16] Hu J Q, Jiang Y, Meng X M, Lee C S and Lee S T 2005 *Small* **1** 429
[17] Fang X S, Ye C H, Zhang L D, Wang Y H and Wu Y C 2005 *Adv. Funct. Mater.* **15** 63
[18] Fang X Y, Ye C H, Peng X S, Wang Y H, Wu Y C and Zhang L D 2003 *J. Mater. Chem.* **13** 3040
[19] Fan H J, Bertram F, Dadgar A, Chirsten J, Krost A and Zacharias M 2004 *Nanotechnology* **15** 1401
[20] Tseng Y K, Huang C J, Cheng H M, Lin I N, Liu K S and Chen I C 2003 *Adv. Funct. Mater.* **13** 811
[21] Chik H, Liang J, Cloutier S G, Koulin N and Xu J M 2004 *Appl. Phys. Lett.* **84** 3376
[22] Xu C X, Sun X W, Dong Z L, Yu M B, My T D, Zhang X H, Chua S J and White T J 2004 *Nanotechnology* **15** 839
[23] Fan H J, Lee W, Scholz R, Dadgar A, Krost A, Nielsch K and Zacharias M 2005 *Nanotechnology* **16** 913
[24] Yao B D, Chan Y F and Wang N 2002 *Appl. Phys. Lett.* **81** 757
[25] Gao P X and Wang Z L 2004 *Appl. Phys. Lett.* **84** 2883
[26] Li Y B, Bando Y, Sato T and Kurashima K 2002 *Appl. Phys. Lett.* **81** 144
[27] Kong Y C, Yu D P, Zhang B, Fang W and Feng S Q 2000 *Appl. Phys. Lett.* **78** 407
[28] Jie J, Wang G, Han X, Yu Q, Liao Y, Li G and Hou J G 2004 *Chem. Phys. Lett.* **387** 466
[29] Fang X S, Ye C H, Zhang L D, Li Y and Xiao Z D 2005 *Chem. Lett.* **34** 436
[30] Yang R, Ding Y and Wang Z L 2004 *Nano Lett.* **4** 1309
[31] Kong X Y, Ding Y, Yang R S and Wang Z L 2004 *Science* **303** 1348
[32] Lao J Y, Wen J G and Ren Z F 2002 *Nano Lett.* **2** 1287
[33] Zhang J, Yang Y D, Jiang F H, Xu B L and Li J P 2005 *J. Solid State Chem.* **178** 2804
[34] Burmeister F, Schäfle C, Matthes T, Böhmisch M, Boneberg J and Leiderer P 1997 *Langmuir* **13** 2983
[35] Fan H J *et al* 2006 *Small* **2** 561
[36] Rybczynski J, Banerjee D, Kosiorek K, Giersig M and Ren Z F 2004 *Nano Lett.* **4** 2037
[37] Banerjee D, Rybczynski J, Huang J Y, Wang D Z, Kempa K and Ren Z F 2005 *Appl. Phys.* A **80** 749
[38] Fan H J, Fleischer F, Lee W, Nielsch K, Scholz R, Zacharias M, Gösele U, Dadgar A and Krost A 2004 *Superlatt. Microstruct.* **36** 95
[39] Wang X, Summers C J and Wang Z L 2004 *Nano Lett.* **4** 423
[40] Xu C X, Sun X W, Chen B J, Dong Z L, Yu M B, Zhang X H and Chua S J 2005 *Nanotechnology* **16** 70
[41] Kuykendall T, Pauzauskie P J, Zhang Y, Goldberger J, Sirbuly D, Den-linger J and Yang P 2004 *Nat. Mater.* **3** 524
[42] Ding Y, Kong X Y and Wang Z L 2004 *Phys. Rev.* B **70** 235408
[43] Zou K, Qi X Y, Duan X F, Zhou S M and Zhang X H 2005 *Appl. Phys. Lett.* **86** 013103
[44] Cheng B, Xiao Y, Wu G and Zhang L 2004 *Adv. Funct. Mater.* **14** 913
[45] Fan H J, Scholz R, Kolb F M and Zacharias M 2004 *Appl. Phys. Lett.* **85** 4142
[46] Fan H J, Scholz R, Kolb F M, Zacharias M, Gösele U, Heyroth F, Eisenschmidt C, Hempel T and Christen J 2004 *Appl. Phys.* A **79** 1895
[47] Manna L, Milliron D J, Meisel A, Scher E C and Alivisatos A P 2003 *Nat. Mater.* **2** 382
[48] Wander A, Schedin F, Steadman P, Norris A, McGrath R, Turner T S, Thornton G and Harrison N M 2001 *Phys. Rev. Lett.* **86** 3811
[49] Meyer B and Marx D 2003 *Phys. Rev.* B **67** 035403
[50] Nguyen P, Ng H T, Yamada T, Smith N K, Li J, Han J and Meyyappan M 2004 *Nano Lett.* **4** 651
[51] Schmidt V, Senz S and Gösele U 2005 *Nano Lett.* **5** 931
[52] Kar S, Bisws S and Chaudhuri S 2005 *Nanotechnology* **16** 3074
[53] Kim K J and Park Y R 2001 *Appl. Phys. Lett.* **78** 475
[54] Scott J F 1970 *Phys. Rev.* B **2** 1209
[55] Zhang X T, Liu Y C, Zhang L G, Zhang J Y, Lu Y M, Shen D Z, Xu W, Zhong G Z, Fan X W and Kong X G 2002 *J. Appl. Phys.* **92** 3293
[56] Ng H T, Chen B, Li J, Han J, Meyyappan M, Wu J, Li S X and Haller E E 2003 *Appl. Phys. Lett.* **82** 2023
[57] Zalamai V V, Ursaki V V, Rusu E V, Arabadji P, Tiginyanu I M and Sirbu L 2004 *Appl. Phys. Lett.* **84** 5168